

**UNIVERSITY OF BUCHAREST
FACULTY OF CHEMISTRY
DOCTORAL SCHOOL IN CHEMISTRY**

**PhD THESIS
ABSTRACT**

**ADVANCED DENITRIFICATION OF WATER BY PALLADIUM
SUPPORTED ON MESOPOROUS MATERIALS**

PhD student:
Simona-Bianca TRONCEA (GHIMIS)

Supervisor:
Prof. Dr. Vasile PARVULESCU

Doctoral committee:

President: Prof. Dr. Camelia BALA

Supervisor: Prof. Dr. Vasile PARVULESCU

Official referents:

1., from
2., from
3., from

2020

Table of content (corresponding to the PhD thesis)

Chapter I: Bibliographical study.....	5
I.1. Introduction.....	5
I.1.1. Water pollution.....	5
I.1.2. Nitrate removal from the groundwater.....	7
I.1.3. Technologies to remove nitrates/nitrites from water.....	9
I.2. Catalytic reduction of nitrates/nitrites.....	11
I.2.1. Catalysts for the water denitrification.....	12
Monometallic catalysts.....	12
Bimetallic Catalysts.....	15
I.2.2. Factors that influence the catalytic reduction process.....	22
pH Influence.....	24
I.2.3. Reaction mechanisms in the removal of the nitrates from water.....	26
I.3. Catalysts supports.....	33
I.3.1. Ordered Mesoporous materials.....	33
I.3.1.1. Classification of mesoporous materials as a function of the chemical composition.....	35
I.3.3. Methods of the synthesis of the mesoporous materials.....	39
I.3.3.1. Evaporation Self Assembly Method (EISA).....	42
I.3.3.2 Coprecipitation method.....	48
References.....	56
Chapter II: Experimental techniques.....	59
II.1.Physico-chemical characterization.....	59
II.1.1. Structural/bulk and surface analysis of the catalysts.....	59
II.1.1.1. Elemental Analysis by Inductively Coupled Plasma-Atomic Emission Spectroscopy (ICP-AES).....	59
II.1.1.2. N ₂ adsorption-desorption measurements.....	60
II.1.1.3. Thermogravimetric analysis.....	64
II.1.1.4. Wide and small angle X-ray diffraction.....	67
II.1.1.5. Temperature-programmed reduction (H ₂ -TPR).....	68
II.1.1.6. Raman Spectroscopy.....	71
II.1.1.7. X-ray photoelectron spectroscopy (XPS).....	75
II.1.1.8. Time-of-Flight Secondary Ion Mass Spectrometry (ToF-SIMS).....	76

II.1.1.9. Microscopy (SEM, TEM)	79
II.1.1.10. H ₂ Chemisorption	81
II.2. Kinetic investigation of the denitrification reaction	83
II.3. Operational analytic conditions	90
II.3.1. Experimental setup and protocols	90
II.3.2. Reaction products analysis	92
II.3.2.1 Anion exchange chromatography	92
II.3.2.2 Cation exchange chromatography	93
Chapter III: Synthesis of the catalytic support	97
III.1. Synthesis of Ce _x Zr _{1-x} O ₂ via the Evaporation Self Assembly Method	97
III.1.1. Introduction	97
III.1.2. Experimental	100
III.1.2.1. Synthesis of the catalytic support	100
III.1.2.2. Catalyst characterization	101
III.1.3. Results and discussion	102
Optimization of the solvent evaporation conditions	102
III.1.3.2. Optimization of the drying conditions	107
III.1.3.3. Optimization of the calcination step	111
III.1.4. Conclusions	114
Chapter IV. Support-induced effect on the catalytic properties of Pd particles in water denitrification : Impact of surface and structural features of mesoporous ceria-zirconia support	116
IV.1. Introduction	116
IV.2. Experimental	118
IV.2.1. Catalyst preparation	118
IV.2.1.1. Ce _{0.5} Zr _{0.5} O ₂ support materials	118
IV.2.1.2. Impregnated Pd/Ce _{0.5} Zr _{0.5} O ₂ catalysts	118
IV.2.2. Physicochemical characterization	119
IV.2.2.1. Bulk characterization	119
IV.2.2.2. Surface characterization	119
IV.2.3. Catalytic measurements	120
IV.3. Results and discussion	120
IV.3.1. Influence of the synthesis route of Ce _{0.5} Zr _{0.5} O ₂ on the physicochemical properties: Structural vs. textural properties	120

IV.3.1.1. Thermal decomposition of the solid precursors of the Ce-Zr mixed oxides prepared by coprecipitation and EISA	120
IV.3.1.2. Structural properties of Ce _{0.5} Zr _{0.5} O ₂ mixed oxides calcined at 400°C	123
IV. 3.1.3. Textural properties of Ce _{0.5} Zr _{0.5} O ₂ mixed oxides calcined at 400°C	126
IV.3.2. Reducibility of bare Ce _{0.5} Zr _{0.5} O ₂ and doped with palladium	128
IV.3.3. Surface properties.....	130
IV.3.4. Catalytic properties of Pd/Ce _{0.5} Zr _{0.5} O ₂ in the reduction of nitrite by hydrogen.	134
IV.3.4.1. Estimation of initial rates.....	135
IV.3.4.2. Selectivity towards the formation of ammonium ions.....	136
IV.4. Discussions.....	138
IV.5 Conclusions.....	142
References	143
Chapter V. Peculiar kinetic properties of Cu-doped Pd/Ce _x Zr _{1-x} O ₂ in water denitrification :	
Impact of Pd-Cu interaction vs structural properties of Ce _x Zr _{1-x} O ₂	146
V.1. Introduction	146
V.2. Experimental	148
V.2.1. Catalyst preparation of Pd-Cu/Ce _x Zr _{1-x} O ₂	148
V.2.2. Physicochemical characterization.....	148
V.2.2.1. Bulk analysis	148
V.2.2.2. Surface analysis.....	149
V.2.3. Catalytic measurements	149
V.3. Results	150
V.3.1. Impact of the structural properties of Ceria-Zirconia mixed oxide on the catalytic properties of palladium and copper in water denitrification.....	150
V.3.1.1. Nitrate conversion and reaction products distribution on pre-reduced Pd-Cu/CZ.....	150
V.3.1.2. Kinetic analysis	155
V.3.2. Bulk and surface properties of Pd-Cu supported on Ceria-Zirconia: Impact of the preparation procedure of Ce _x Zr _{1-x} O ₂ on the nature of interaction with the metallic phase	157
V.3.2.1. Structural vs. textural properties on Ceria-Zirconia prepared through EISA or co-precipitation method	157
V.3.2.2. TEM and EDS analysis	158
V.3.2.3. Impact of palladium and copper addition on the reducibility	162
V.3.2.4. XPS surface analysis of Pd-Cu/CZ	165

V.3.2.5. ToF-SIMS analysis	169
V.4. Discussion	171
V.4.1. Impact of the oxidative properties of the support on the secondary ammonia oxidation	172
V.4.2. Influence of Palladium and copper loading on the extent of Pd-Cu interaction : Impact on the catalytic properties	173
V.5. Conclusions	174
Reference.....	175
Chapter VI. Kinetics of undesired ammonia production during nitrite reduction on Pd/CeO ₂ -ZrO ₂ : Impact of metal loading and structural features of the support	178
VI.1. Introduction	178
VI.2. Experimental	179
VI.3. Results and discussion	180
VI.3.1. Physicochemical characterization of supported Pd on ceria-zirconia mixed oxide and single CeO ₂ and ZrO ₂ materials.....	180
VI.3.2. Kinetic of nitrites reduction and related production of ammonia	183
VI.3.3. Kinetic modelling	187
VI.4. Conclusions.....	191
Chapter VII. GENERAL CONCLUSIONS.....	193

Introduction

The presence of nitrate in water is presently a common problem across Europe. The catalytic reduction of nitrate has been suggested in the literature as a promising method for its elimination, without the drawbacks of the conventional technologies. This process consists in the reduction of nitrate to nitrogen over bimetallic catalysts in the presence of a reducing agent.

The main objective of this thesis was the study of the catalytic reduction of nitrate in water with hydrogen in a systematic way, testing several metal catalysts and their composition, preparation conditions and supports, focusing on the use of $\text{Ce}_{0.5}\text{Zr}_{0.5}\text{O}_2$ as support, and clarifying some kinetic aspects.

In order to accomplish this objective, the thesis investigated:

- i) the optimization of the synthesis routes of the catalytic supports;
- ii) the characterization of the catalyst by complementary techniques, such as: ICP-AES, BET, TGA, XRD, H_2 -TPR, XPS, TEM, SEM, Raman, Tof-SIMS, H_2 chemisorption analysis and catalytic results;
- iii) the evaluation of the obtained catalysts in water denitration reaction;
- iv) the identification of the denitration reaction products;
- v) the study of the kinetics of the processes.

The Ph. D thesis is structured in two parts: the first part of this work is dedicated to a critical analysis of the reports in the literature (Chapter I) and a short description of the analysis techniques used for the characterization of the materials (Chapter II).

The second part, the next 4 chapters (Chapters III, IV, V, VI) discuss the experimental results and in Chapter VI are presented the general conclusions of the thesis.

Chapter I

The pollution from domestic, agricultural and industrial sources remain a problem, despite the actual progress, because of the directness through discharges or indirectly spreading of nitrogen fertilizers and pesticides through leaching from old landfills or industrial sources. In Europe, only around one third of the groundwater currently exceeds the accepted nitrate limits. Large contents of nitrogen and phosphorus in these waters (including rivers) can lead to eutrophication causing ecological changes. These would contribute to the disappearance of plant and animal species and will have negative impacts on the health of the human being [4,5].

As an example, Figure I.2. illustrates sources of pollution of the aquatic environment by nitrogen.

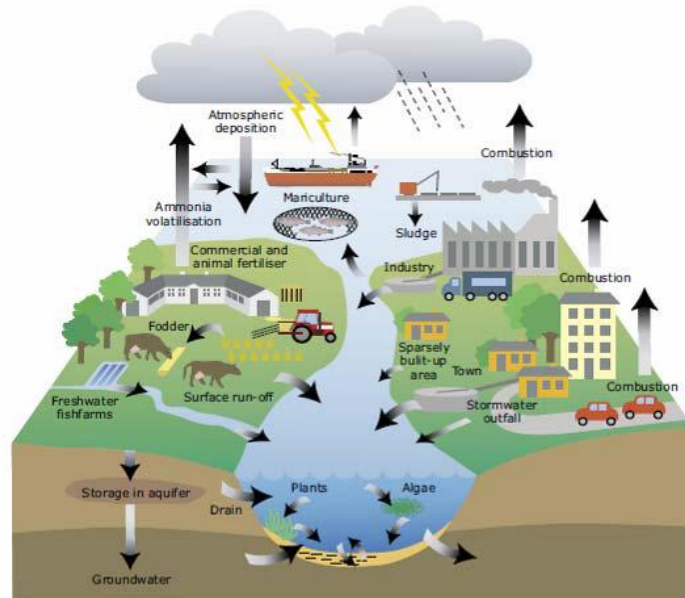


Figure I.2. Sources of pollution of the aquatic environment by nitrogen. [4]

The reduction of nitrate in the presence of hydrogen over a solid catalyst may offer therefore an alternative and economically advantageous process to the biological treatment as a means of purifying drinking water streams. The main drawback of this process is the formation of ammonia as by-product, which is also undesirable in drinking water [4,12,13].

I.2. Catalytic reduction of nitrates/nitrites

The chemical nitrate reduction using a catalyst (catalytic reduction method) was firstly introduced in the late 1980s. Accordingly, in the presence of a catalyst, nitrate is reduced by hydrogen. The main advantage of the catalytic denitration compared to other commercial techniques is the reduced waste management cost. In addition, the process is generally run at room temperature and atmospheric pressure; thus it is an energy efficient process. The technical and economic feasibility of the catalytic hydrogenation of nitrate/nitrite in water was already demonstrated at groundwater sites at a field-scale [16].

World Health Organization established to: $50 \text{ mg/L}^{-1} \text{ NO}_3^-$, $0.5 \text{ mg/L}^{-1} \text{ NO}_2^-$ and $0.5 \text{ mg/L}^{-1} \text{ NH}_4^+$ [16].

The most active and selective catalysts for the nitrate reduction, were considered Pd-Cu, Pd-Sn and Pt-Cu pairs. However they are still lacking in terms of selectivity towards nitrogen.

The methods for the preparation of these catalysts are the impregnation of both metal salts on the support or successive addition of metal salt. For both the preparation methods it is impossible to provide the formation of only bimetallic particles [19].

The use of monometallic catalysts (Pd or Pt) deposited on reducible supports (SnO_2 , TiO_2 , CeO_2 , and pillared clays) using appropriate CO_2 buffering favours the increase of the activity for the reduction of nitrate. In terms of N_2 selectivity, as noble metal component of bimetallic catalysts, palladium and platinum provided similar values. However, the activity for the nitrate reduction was much higher using Pd-based catalysts [33, 37, 38].

It was thus concluded that the nitrate reduction rate and the selectivity for the final products are significantly affected by the dispersion of the particles on the support, the size of the particles and the formation of agglomerates or alloys. These factors, which are strongly dependent on the preparation method, the metal loading and the Pd:Me ratio (Me = Cu, In or Sn), determine the distance between the active sites of palladium and noble metal, influencing the interactions between the reactants and the catalyst.[33]



Figure I.5. Proposed models of Pd and Pd-Cu particles [33,40]

These conclusions support the fact that the optimization of the metal loading and the Pd:Me ratio of the catalysts are very important factors for improving the rate of the catalytic reduction of nitrates.

I.3.3.1. Evaporation Self Assembly Method (EISA)

The so-called EISA method, initially proposed by Brinker and colleagues [62], is the effect of the processes taking place upon the formation of mesostructured silica films. Starting from dilute solutions, a liquid crystalline (LC) mesophase is gradually formed upon the solvent evaporation. The formation of an inorganic network around this LC phase permits the formation of well-defined mesostructured hybrids, which present a segregation of organic and mineral domains at the nanoscale. This procedure permits to avoid the diffusion problems encountered when infiltrating a real LC structure with a metal precursor (Figure I.14., route A). [62]

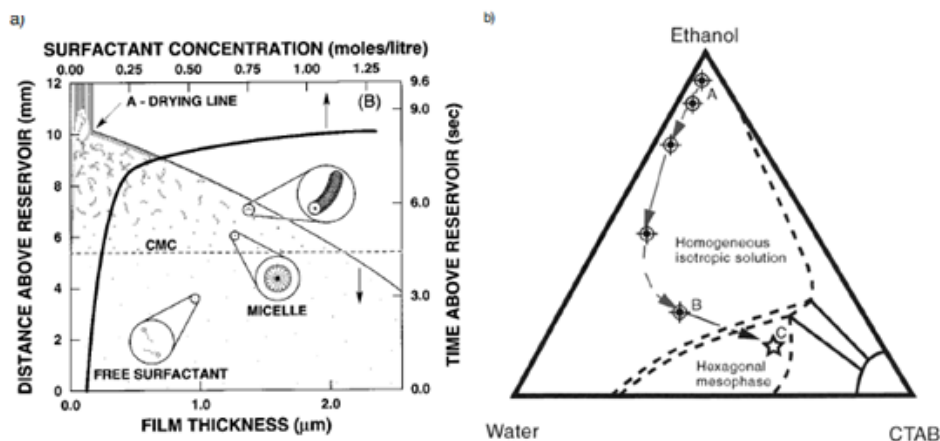


Fig. I.14.. a) Steady-state film thinning profile established during dip-coating of a complex fluid comprising soluble silica, surfactant, alcohol, and water. Initial surfactant concentration $c_0 \ll c_{mc}$. The surfactant concentration increases with the distance above the reservoir surface [74]. b) Approximate trajectory taken in ethanol/water/CTAB phase space during dip-coating. Point A corresponds to the initial composition of entrained solution, Point B is near the drying line, and Point C corresponds to the dried film. Pathway calculated by combining results of in situ probe experiments and imaging ellipsometry and superimposing data onto the experimental phase diagram.[74]

Chapter II: Experimental techniques

A complete characterization of the prepared materials requires a collection of informations from a number of physical, chemical and spectroscopic techniques.

Therefore, an adequate structural and physico-chemical characterization of the catalysts may provide a valuable information for a better understanding of the catalysts behaviour in terms of stability, activity and selectivity. Thus, a wide range of characterisation techniques have been utilized: e.g. i) X-ray diffraction techniques (XRD) (giving information on the dispersion and composition of metal particles in the catalysts and supports); ii) BET method (SBET) (affording the calculation of the specific surface area from the N₂ adsorption isotherms); iii) transmission electron microscopy (TEM) (giving the size distribution of the metallic particles); iv) X-ray fluorescence (giving the metal content and elemental ratios of the catalysts); v) X-ray photoelectron spectra (XPS) (indicating the evolution of the oxidation and chemical state of the active phases, and the binding energy of the different element core levels); vi) CO chemisorption (giving the average metal crystallite diameter and the metal dispersion in the reduced samples from the double isotherm method); vii) H₂ pulse chemisorption measurements (measuring the dispersion of palladium and from the hemispherical model); viii) temperature-programmed reduction of hydrogen (H-TPR) (allowing investigation of the reducibility of the metals in the catalysts)[33].

Chapter III: Synthesis of the catalytic support

The purpose of the research discussed in this chapter was to optimize the synthetic conditions of the mesostructured materials $\text{Ce}_{0.5}\text{Zr}_{0.5}\text{O}_2$ mixed oxides using the evaporation – induced self-assembly method. To make more clear this attempt they were considered three objectives: (a) the optimization of the solvent evaporation conditions, (b) the optimization of the drying process and (c) the optimization of the calcination conditions.

III.1.2. Experimental

III.1.2.1. Synthesis of the catalytic support

Evaporation induced self assembly method (EISA) is a method that affording a phase and pore size control and a good crystallinity of materials. The preparation experiments used a volatile solvent with the capability to delay both the hydrolysis and condensation rates of the metal species. Such a behaviour is highly recommended for the formation of ordered mesostructures. By the evaporation of the solvent, the surfactant becomes highly concentrated leading to a liquid-crystal incorporating the inorganic species and finally to ordered composite mesostructures [24]. Controlling this important step allows to improve the textural properties of the targeted mixed oxides. The inorganic framework is then solidified via a post-treatment. The last step of the process is the removal of the polymer by calcination. Mixed metal oxides with open pores can be thus generated.

The synthesis started by dissolving 0.5 g of Pluronic P123 ($M_{av}=5800$, EO20PO70EO20, Aldrich) in 10 ml of ethanol. Then, quantitative $\text{CeNO}_3 \cdot 6\text{H}_2\text{O}$ (Sigma Aldrich) and $\text{ZrOCl}_2 \cdot 8\text{H}_2\text{O}$ (Sigma Aldrich) were added (the concentration of the Ce and Zr was 5mmol), in order to produce a mixed oxide with an atomic Ce:Zr ratio of 1:1. After stirring for 3h at room temperature, the homogeneous sol was transferred to an oven under desired temperature and humidity:

- temperature: 40°C, relative humidity:

S1(40%rH), S2(50%rH), S3(70%rH)

The solvent evaporation have been carried out in a climate chamber. After 48 h ageing, the gel product was dried at 100°C for 24 h. After 48 h aging, the gel product was dried at different temperatures. Accordingly the samples were denoted as:

S2. 1.- 60°C, 24h,

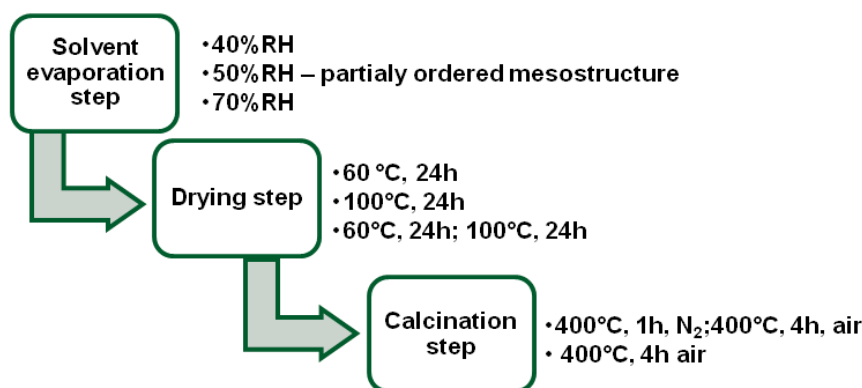
S2. 2.- 100°C, 24h,

S2. 3.- 60°C, 24h; 100°C, 24h

The calcination was carried out by increasing the temperature from room temperature to 400°C with a ramp of 1°C min⁻¹. After reaching 400°C this temperature was maintained for another 4h in air.

The resulted solids were labeled as Ce_{0.5}Zr_{0.5}O₂ S1(40%rH), Ce_{0.5}Zr_{0.5}O₂ S2(50%rH) and Ce_{0.5}Zr_{0.5}O₂ S3(70%rH), respectively. The parameters of the entire process are described in Scheme III.1.

Scheme III. 1. EISA synthesis steps



According with the processes describe in this chapter, we selected as optimal conditions for the synthese of catalytic support, the next conditions:

- For the solvent evaporation step 50%rH, for 48 h, in a climate chamber;
- For drying step 60 °C ,24 and 100 °C, 24h;
- For calcinations step, 400⁰C, in air, for 4h.

The small angle XRD analysis of the dried supports results evidence the presence of the partially ordered mesostructured for the supports synthesized by using method EISA, contrary to the same supports synthesized by using classical coprecipitation method. Concerning the optimization route, drying steps were also important and the solvent evaporation step was finded as: 60 °C ,24 and 100 °C, 24h. After calcination at 400⁰C, in air, for 4h, the partially ordered structured is maintained. These supports will be impregnated and utilized as catalyst for the water denitration reaction, as we can see in the next chapters.

Chapter IV. Support-induced effect on the catalytic properties of Pd particles in water denitration : Impact of surface and structural features of mesoporous ceria-zirconia support

This chapter reports the influence of the support materials on the catalytic properties of Pd particles in the reduction of nitrites in aqueous phase performed at 20°C. Ceria-zirconia mixed oxide (Ce_{0.5}Zr_{0.5}O₂) as support was prepared according to co-precipitation and evaporation-induced self-assembly methods and then calcined in air at 400°C. Straight forward bulk and surface characterizations showed a preferential tetragonal structure for the

mixed-oxide prepared from the EISA method exhibiting a surface zirconium enrichment whereas the co-precipitation method leads to strong inhomogeneity in composition with the segregation of the fluorite structure of CeO₂ coexisting with the mixed oxide. As a consequence some significant deviations are observed on the surface composition with surface cerium enrichment corresponding to a greater formation of anionic vacancies reflected by higher Ce³⁺/Ce⁴⁺ ratio on sample reduced at 300°C. Such structural changes have also some consequence on the textural properties with monomodal pores size distribution on CZ(EISA) whereas the CZ(COP) is characterized by a bimodal distribution with larger pores likely associated to the formation of CeO₂. All those changes can alter the impregnation of palladium which was found more poorly dispersed on CZ(COP) irrespective of the reduction temperature, i.e., 300°C or 500°C under pure hydrogen.

IV.2.1.1. Ce_{0.5}Zr_{0.5}O₂ support materials

Ce_{0.5}Zr_{0.5}O₂ was prepared according to two different experimental protocols. The first method EISA method was described in Chapter III. For the second protocol, the co-precipitation method (COP), Ce(NO₃)₃·6H₂O and ZrOCl₂·8H₂O were dissolved in distilled water under magnetic stirring and then heated at 60°C. Cerium and zirconium hydroxides were precipitated by adding dropwise ammonia solution up to pH = 10 and the suspension was stirred for 4 hours. The solid precursor was washed with distilled water several times before aging at room temperature for 48 hours, and drying at 120°C for 24 hours[23].

The solid oxy-hydroxide precursors obtained through these two methods were calcined in air at 400°C for 4 hours. The temperature gradually increased with a gradient temperature of 1°C/min.

IV.2.1.2. Impregnated Pd/Ce_{0.5}Zr_{0.5}O₂ catalysts

The monometallic catalysts were prepared by incipient wetness impregnation from aqueous solutions of palladium nitrates (Pd(NO₃)₂·2H₂O, Sigma Aldrich) with concentration adjusted to get 2.3 wt.% or 0.46 wt.%Pd [24]. After impregnation, the precursors were dried in air at 105°C overnight, calcined in air at 400°C for 2 hours and finally reduced in pure hydrogen at 300°C or 500°C for 4 hours with a heating rate of 5°C/min and a H₂ flow of 60 mL.min⁻¹. The reduced catalysts were finally labeled xPd/CZ(EISA) and xPd/CZ(COP) where x stands for the weight palladium loading equal to 0.46 or 2.3 wt.%.

IV.2.3. Catalytic measurements

The nitrite reduction reaction was performed in a 250 mL batch reactor equipped with a magnetic stirrer operating at atmospheric pressure. 80 or 400 mg of catalyst in powder form, with average grain size of 250µm, were introduced in the reactor and then purged with

pure H₂ for 1 hour at RT. In the second stage, 40 mL of ultrapure water was added to the system under a flow of H₂ (200 mL/min) for 1 hour. Afterwards, 10 mL of nitrites solution (500 mg/L or 100 mg/L) were introduced and the suspension was stirred with a rotation speed set at 700 rpm. The experiment was carried out at 20°C with a H₂ flow rate of 200 mL/min. Nitrite concentration was monitored by an ionic chromatograph (Metrohm 844 UV/VIS Compact IC–Column Metrosep A Supp 16-250/4.0). The concentration of ammonium ions were measured by using an ion chromatograph (Metrohm 861 Advanced Compact IC – column Metrosep C 6 -250/4.0).

IV.3.4. Catalytic properties of Pd/Ce_{0.5}Zr_{0.5}O₂ in the reduction of nitrite by hydrogen

IV.3.4.2. Selectivity towards the formation of ammonium ions

Significant information is also related to the selectivity behavior of Pd/CZ samples with the formation of undesired products such as ammonia. As shown in Fig. IV 14, Pd/CZ behaves differently mimicking the selectivity recorded on Pd/CeO₂ with a volcano type curve suggesting the occurrence of sequential processes involving the formation and the consumption of ammonia. Additional information relative to the involvement of sequential processes can be obtained : – (i) Ammonium ions concentration gradually decreases while nitrites are completely converted as exemplified on 0.46Pd/CZ(EISA) which could rule out an hypothetical direct redox reaction between NH₄⁺ and NO₂⁻ contrarily to previous assumptions [63]. – (ii) Qualitatively, the sequential consumption of ammonium ions seems to occur more readily on sample reduced at 500°C by comparing the ammonium concentration at the maximum and at the end after 6 hours reaction. As exemplified, this sequential reaction process does not occur significantly on 0.46Pd/CZ(COP) reduced at 300°C.

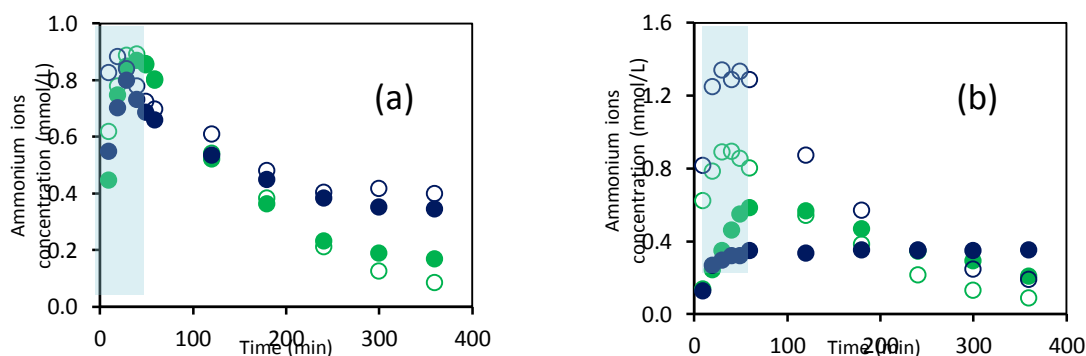


Fig. IV. 14. Influence of the palladium loading and reduction temperature on the concentration profiles of ammonium ions vs. time formed during the reduction of nitrites by hydrogen in batch conditions : (a) on Pd/CZ(EISA) and (b) Pd/CZ(COP) – full symbol reduction at 300°C, open symbol reduction at 500°C – 0.46 wt%Pd in blue and 2.3 wt.% Pd in green.

Table IV. 3. Initial rate measurements performed at 20°C on Pd/Ce_{0.5}Zr_{0.5}O₂ (0.46Pd/CZ and 2.3Pd/CZ) during the reduction of nitrite to nitrogen.

Catalyst	T _{Red.} (°C)	d _{Pd} (nm)	Initial rate (mol.h ⁻¹ .g _{Pd} ⁻¹)	TOF (h ⁻¹)	Interfacial rate (10 ⁻¹² .μmol.s ⁻¹ .cm ⁻¹)	NH ₄ ⁺ ^a at max	NH ₄ ⁺ ^b at the end
end							
2.3Pd/CZ(EISA)	300	6.1	5.0×10 ⁻²	29.3	8.4	15.8	3.0
2.3Pd/CZ(COP)	300	10.9	4.6×10 ⁻²	47.6	24.2	10.5	3.5
0.46Pd/CZ(EISA)	300	8.6	11.6×10 ⁻²	95.2	38.2	14.2	6.2
0.46Pd/CZ(COP)	300	10.2	1.9×10 ⁻²	33.8	30.3	6.1	6.3
2.3Pd/CZ(EISA)	500	19.9	3.4×10 ⁻²	64.4	75.1	16.0	1.7
2.3Pd/CZ(COP)	500	49.3	3.7×10 ⁻²	175.9	499	16.0	1.7
0.46Pd/CZ(EISA)	500	31.7	15.8×10 ⁻²	474.6	886	15.4	7.0
0.46Pd/CZ(COP)	500	30.1	2.6×10 ⁻²	74.0	130	24.0	3.3

^aAmmonia concentration formed at maximum expressed in mg/L

^b Residual ammonia concentration formed at the end of the reaction expressed in mg/L

As demonstrated in this chapter, the implementation of different methods for the preparation of Ce_{0.5}Zr_{0.5}O₂ can lead to solids exhibiting different bulk and surface properties which can potentially influence the nature and the extent of interactions with palladium. In terms of structural properties, the Evaporation Induced Self-Assembly method leads mainly to the stabilization of the tetragonal structure for ceria-zirconia mixed oxides with no detectable inhomogeneity in bulk composition. As shown, the normalized rate expressed per gram of palladium provide an overall information which undoubtedly show the superiority of 0.46Pd/CZ(EISA) reduced at the lowest temperature, i.e., 300°C, which formally is not helpful to differentiate the particle size dependency or the role played by the metal-support interface. Surprisingly the normalized rate expressed per gram of palladium measured on reduced samples at 500°C are comparable still verifying the highest performances of 0.46Pd/CZ(EISA) while at higher reduction temperature an increase of the density of anionic vacancies jointly to a greater metallic character should enhance the reaction rate [14].

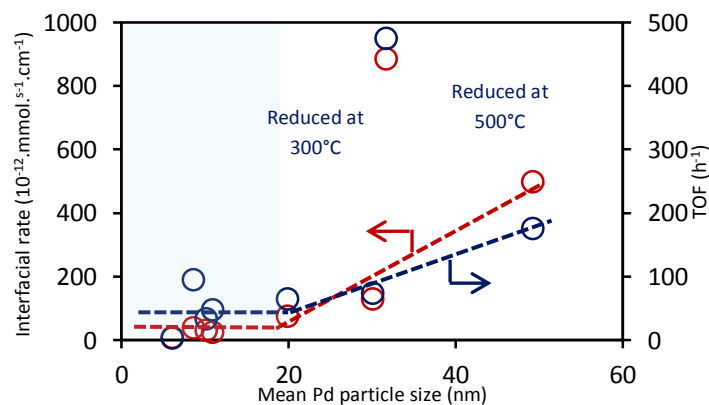


Fig. IV.15. Comparison of TOF and interfacial rates vs. mean Pd particle size on Pd/CZ

IV.5 Conclusions

Catalytic measurements show a faster reduction of nitrates on samples reduced at 500°C with a prominent production of ammonia at the early stage of the reaction at the expense of nitrogen the target molecule. Unprecedented selectivity behavior is observed with a sequential ammonia consumption promoted on Pd/Ce_{0.5}Zr_{0.5}O₂ irrespective of the preparation route. The changes observed in the reaction rates are strongly dependent on the pre-reduction leading to significant enhancements when the pre-reduction is performed at 500°C. The comparison of TOF and interfacial rates expressed per cm, reflecting the length of the perimeter of metallic Pd particles, versus the particle size does not provide clear evidence to privilege the prevalence of structural or electronic factors which could govern the catalytic properties but highlight the superiority of 0.46Pd/CZ(EISA) compared to all other samples. However, it seems that there is no strong evidence that the support materials would directly participate to the reaction especially on the EISA support stabilizing a tetragonal structure known for exhibiting lower redox properties than the cubic form. This seems in relative good agreement with previous investigation that showed nitrite reduction would occur through classical mechanism involving only metallic sites, the involvement of oxygen vacancies being more obvious for the reduction of nitrates to nitrites.

Chapter V. Peculiar kinetic properties of Cu-doped Pd/Ce_xZr_{1-x}O₂ in water denitration : Impact of Pd-Cu interaction vs structural properties of Ce_xZr_{1-x}O₂

The overall objective of this chapter was to investigate the nature of the interactions between Cu and Pd, at low and high metal loading, on the catalytic reduction of nitrates by H₂ with CeO₂-ZrO₂ mixed oxides as support material. Conventional co-precipitation and more innovative evaporation-induced self-assembly method for the preparation of CeO₂-ZrO₂ can lead to different structural and textural features [27] that could *a priori* modify the nature of the interactions with Pd and Cu. The consequences on the kinetics will be discussed in this chapter.

V.2. Experimental

The catalysts are prepared accordingly the previous chapters.. Also the catalytic measurements are described in chapter IV.

V.3.1.1. Nitrate conversion and reaction products distribution on pre-reduced Pd-Cu/CZ

As observed in Table V.1., the preparation route of the support material (EISA vs. coprecipitation method) and the palladium loading influence the catalytic properties with higher normalized rate on 1Pd/CZ(EISA).

Table V. 1. Kinetic features of Pd/Ce_{0.5}Zr_{0.5}O₂ (0.46Pd/CZ and 2.3Pd/CZ) during the reduction of nitrite by H₂O from ref. [1].

Catalyst	T _{Red.} (°C)	Initial rate (mol.h ⁻¹ .g _{Pd} ⁻¹)	TOF (h ⁻¹)	NH ₄ ⁺ concentration (μmol.L ⁻¹)	
				at max ^a	at the end ^b
5Pd/CZ(EISA)	300	5.0×10 ⁻²	29.3	929	176
5Pd/CZ(COP)	300	4.6×10 ⁻²	24.2	617	206
1Pd/CZ(EISA)	300	11.6×10 ⁻²	38.2	825	365
1Pd/CZ(COP)	300	1.9×10 ⁻²	30.3	359	370

^a Ammonia concentration formed at the maximum

^b Residual ammonia concentration formed at the end of the reaction

By examining the concentration profile of ammonium ions, different regimes are observable as a function of the progress of the reaction. Indeed, a much faster production of ammonia occurs at the early stage of the reaction on 5Pd-1Cu/CZ(EISA) than on 5Pd-1Cu/CZ(COP) which could be assigned to a greater number of electron-rich active metal states as already pointed out [21] in agreement with a strengthening of the metal-support interaction. Intriguingly, 5Pd-1Cu/CZ(EISA) exhibit a peculiar kinetic behavior related to a sharp drop of ammonia concentration leading to the lowest residual concentration value after 6h reaction, *i.e.* 187 ppm. Similar observations also characterize 5Pd-1Cu/CZ(COP) but in lower extent, the residual ammonia concentration stabilizing near 331 ppm. Such comparison underlines the occurrence of secondary reaction involving ammonia. It is worthwhile to note that the opposite trend characterizes low loaded Pd and Cu catalysts. Interestingly, a successive consumption of ammonia is not observed on 1Pd-0.2Cu/CZ(EISA) whereas it occurs significantly on 1Pd-0.2Cu/CZ(COP) correlated to a stabilization of nitrites concentration and suggesting that ammonia could be re-oxidized preferentially into N₂ on the series Pd-Cu/CZ(EISA) and nitrites on Pd-Cu/CZ(COP).

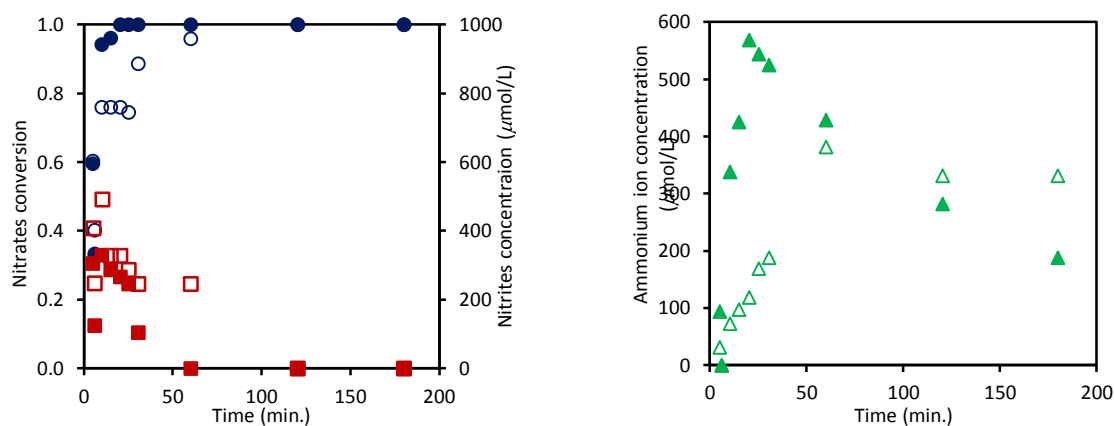


Fig. VI.1. Catalytic properties of 5Pd-1Cu/CZ(EISA) (full symbols) and 5Pd-1Cu/CZ(COP) (empty symbols) pre-reduced at 300°C: Nitrate conversion (circle); Nitrites concentration (square); ammonium concentration (triangle).

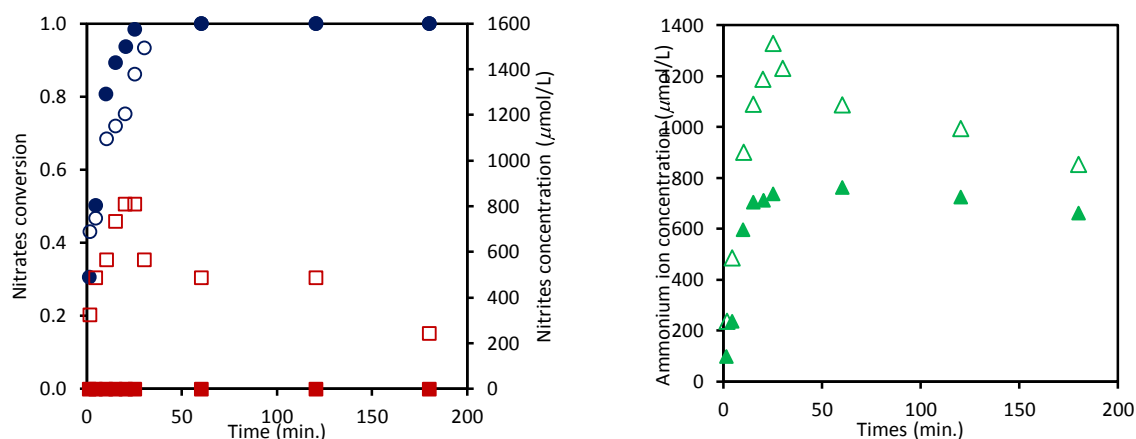


Fig. VI. 2. Catalytic properties of 1Pd-0.2Cu/CZ(EISA) (full symbols) and 1Pd-0.2Cu/CZ(COP) (empty symbols) pre-reduced at 300°C: Nitrate conversion (circle); Nitrites concentration (square); ammonium concentration (triangle)

V.3.1.2. Kinetic analysis

The kinetics of the overall reduction of nitrates has been studied in order to get more insight into the specific role played by copper and palladium and their potential interactions that could altered their intrinsic catalytic properties. As afore mentioned, the overall reduction of nitrates can be regarded asa two-step reaction processthrough theproduction of nitrites and their subsequent consumption according to the following sequential reaction mechanism: $\text{NO}_3^- \xrightarrow{k_1} \text{NO}_2^- \xrightarrow{k_2} \text{hydrogenated products (N}_2 \text{ and NH}_3\text{)}$. In this sequence, we did not consider side reactions involving the potential re-oxidation of ammonia to nitrites and nitrogen. One can hypothesize a pseudo first order kinetics for nitrates and nitrites reduction in agreement with earlier investigations[29-31]which makes easier the resolution of the first order differential Eq. (4).

$$\frac{d[\text{NO}_2^-]_t}{dt} = k_1[\text{NO}_3^-]_t - k_2[\text{NO}_2^-]_t \quad (4)$$

with $[\text{NO}_3^-]_t = [\text{NO}_3^-]_0 \exp(-k_1 t)$ (5)

The rate constant k_1 in Table 3 can be estimated from Eq. (5) by using nitrate concentration measured vs. time in Figs. 1 and 2. As observed the highest values still characterized the series Pd-Cu/CZ(EISA). The integration of Eq. (4) leads to Eq. (6) theoretically suited to describe the evolution of the nitrites concentration vs. time. A seen a maximum usually appears corresponding to a derivative almost nil which leads to (Eq. (7)) and allows a rough estimation of the rate constant k_2 .

$$[\text{NO}_2^-]_t = \frac{k_1[\text{NO}_3^-]_0}{k_2 - k_1} [\exp(-k_1 t) - \exp(-k_2 t)] \quad (6)$$

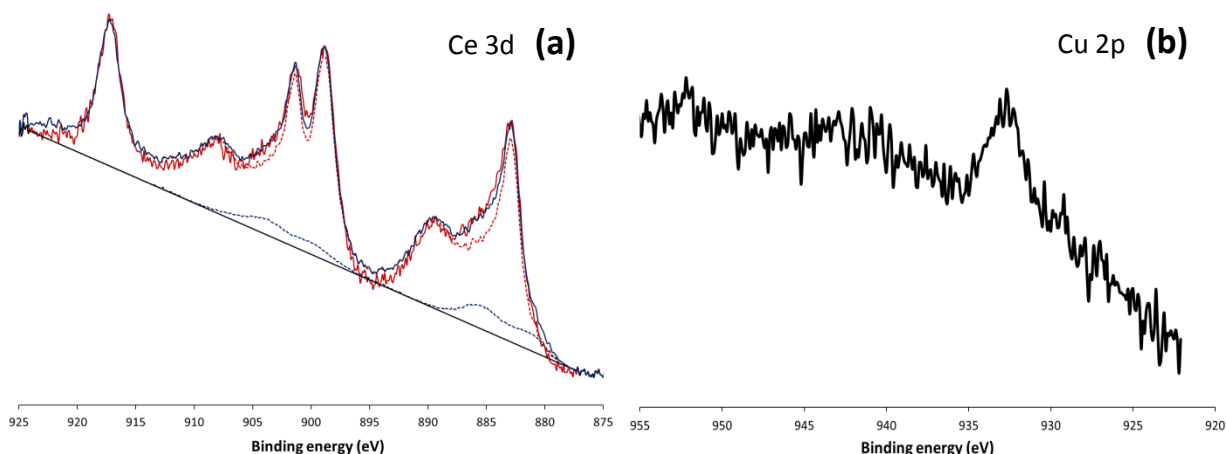
$$t_{\text{opt}} = \frac{\ln k_1/k_2}{(k_1 - k_2)} \quad (7)$$

k_1 and k_2 values obtained through this method can be used as inlet values for a subsequent statistical optimization according to a classical least square method. The optimized rate constant values obtained when $\Sigma(r_{\text{exp}} - r_{\text{cal}})^2$ tends to a minimum are reported in Table 3. As seen, those kinetic parameters do not invalidate the normalized rates previously estimated but clarify the specific role of copper and palladium in the overall reduction process. It seems obvious that the values for k_1 are not sensitive to the copper loading and related changes in Cu dispersion since the reduction of nitrates is recognized as weakly structure sensitive. The lower value obtained on Pd-Cu/CZ(COP) could be equally explained by a more extensive copper oxidation which suggests weaker interactions with Pd or the support to protect the metallic character of copper. The rate constant k_2 is expected much higher than k_1 on 1Pd-0.2Cu/CZ(EISA) because nitrites species have not been detected. On the other hand only slight difference between k_1 and k_2 are discernible for the three other samples.

V.3.2.4. XPS surface analysis of Pd-Cu/CZ

XPS measurements were performed on calcined samples. The characteristic Zr 3d, Ce 3d, O1s, Pd 3d and Cu 2p core levels were investigated. The binding energy values near ~182.3 eV for the Zr3d_{5/2} photopeak characterize the presence of Zr⁴⁺. As earlier discussed, the complexity of Ce 3d photopeak is connected to different components their decomposition giving rise to the relative concentration of Ce³⁺ and Ce⁴⁺[23]. The spectral decomposition depicted in Fig.V. 10(a) reveal the prevalence of Ce⁴⁺ on calcined samples. Indeed, the

estimates for the $Ce^{3+}/Ce^{3+}+Ce^{4+}$ never exceed 0.08. Indeed, the decomposition of the Pd $3d_{5/2}$ on this latter catalyst highlights two components at 337.7 eV and 339.1 eV. It is worthwhile to note that higher B.E. values did not appear on calcined 5Pd/CZ(COP). This contribution appearing near 339.1 eV has been already observed and ascribed to Pd^{4+} and/or PdO_y with $1 < y < 2$ [42-46]. In fact, different origins can explain the development of high B.E. contributions related to electron transfer monitored by the extent of interaction with the support, with copper and/or by the particle size then stabilizing the electron deficient $Pd^{\delta+}$ species with $\delta > 2$. The Cu $2p_{3/2}$ photopeak gives rise to a distinct signal only on 5Pd-1Cu/CZ(EISA) corresponding to a B.E. value of 932.7 eV. The characteristic shake up structure range 940-950 eV evidences the presence of Cu^{2+} (see Fig. V. 10(b)). Nevertheless, the abnormally low B.E. can suggest the coexistence of oxidic copper species stabilized in a lower oxidation state as already pointed out on bimetallic Pd-Cu systems [47,48]. At a first glance, this observation could be in connection with the appearance of the high B.E. contribution on the Pd $3d_{5/2}$ near 339.1 eV then reflecting an electron donation from Pd to Cu thanks to a closer interaction between these two elements in calcined 5Pd-1Cu/CZ(EISA). For low loaded Pd-Cu/CZ samples, the weak intensity of the Pd 3d photopeak and a significant overlapping between Zr 3d and Pd 3d photopeaks make difficult any accurate quantitative analysis. Unfortunately, the examination of the Cu 2p core level did not lead to detectable copper species. Particular attention was paid to the photopeak Pd 3d, Cu 2p and Ce 3d. XPS photopeaks recorded on 5Pd-1Cu/CZ(EISA) are reported in Fig. V. 10.



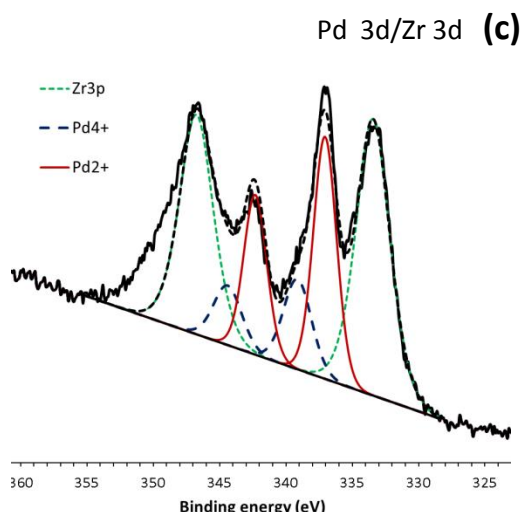


Fig. V.10. An example of Ce 3d (a), Cu 2p (b) and Pd 3d photopeak on calcined 5Pd-1Cu/CZ(EISA).

As illustrated, the envelopes corresponding to the sum of the components u, u', u'', u''' (dotted red line) and v, v', v'', v''' (dotted blue line) assigned to Ce^{4+} and Ce^{3+} respectively show that most of cerium is stabilized as Ce^{4+} the atomic fraction of Ce^{3+} being less than 8%. Such tendency was usually observed on all calcined samples irrespective of Pd and Cu loading. Copper was only detected on 5Pd-1Cu/CZ(EISA). As seen on the Pd 3d photopeak (see Fig. V. 10(c)) a significant overlapping of the Zr 3p is observable in most cases only one component on the Pd $3d_{5/2}$ was observed except on 5Pd-1Cu/CZ(EISA). As shown, the peak decomposition, illustrated in Fig.V.10(c), reveals two components at 337.7/339.1 eV ascribed to Pd^{2+} and Pd^{4+} . The examination of the surface concentration clearly indicates significant surface palladium enrichment on 5Pd-1Cu/CZ irrespective of the protocol use for the preparation of ceria-zirconia mixed oxide. Interestingly, copper is only detected on 5Pd-1Cu/CZ(EISA) which leads to a slightly lower surface atomic Pd/Cu ratio compared to elemental analysis. Such observation does not indicate significant deviation between bulk and surface composition according to the margin of error. Useful information arises from the comparison of Zr/Ce ratio from XPS and elemental analysis. It is obvious that a sharp surface Ce enrichment occurs on the series Pd-Cu/CZ(COP) especially on 1Pd-0.2Cu/CZ(COP).

V.3.2.5. ToF-SIMS analysis

Time of Flight-Secondary Ion Mass Spectrometry (ToF-SIMS) can detect molecular secondary ions and then provide unique information on the coordination of elements. Hundreds of cluster ions were collected on calcined 5Pd-1Cu/CZ and spectra were particularly complex to assign due to a high number of isotopes for zirconium (5 isotopes) and palladium (6 isotopes) producing a lot of possible overlappings. In this context, a particular attention was paid to the detection of mixed oxide clusters containing Pd, Cu and O

or Ce, Cu and O and their evolution on calcined and reduced samples because they reflect the close proximity of Pd and Cu in the same nano-sized aggregates. We managed to detect PdOCu cluster ions in the positive mode. Assignments were confirmed by the detection of $^{104}\text{PdOCu}^+$, $^{105}\text{PdOCu}^+$, $^{106}\text{PdOCu}^+$ and $^{108}\text{PdOCu}^+$ molecular ions in the spectra with intensities in accordance to the natural isotopic ratios. Fig.V.11 reports the evolution of PdOCu⁺ intensity on calcined and *ex situ* reduced 5Pd-1Cu/CZ(EISA) and 5Pd-1Cu/CZ(COP). A comparison can be established with the benchmark 5Pd/CZ(EISA) and 5Pd/CZ(COP). As a general trend, the contribution on mass spectra of the PdCuO⁺ cluster ions appears more distinctly on the series 5Pd-1Cu/CZ(EISA) especially of reduced samples at 300°C. We checked the same trend in Fig.V.12 on samples reduced at 500°C. The opposite observation is noticeable on 5Pd-1Cu/CZ(COP) while the intensity fragment is observable on the calcined sample, a strong attenuation is clearly observed in the reduced samples. This trend is also confirmed when catalyst samples are reduced at 500°C (see Fig. 12) showing that the fragment assigned to PdCuO⁺ cluster ions strongly attenuates on 5Pd-1Cu/CZ(COP).

Among the different cluster ions identified, none of them corresponded to association between copper ceria and oxygen which could suggest a close proximity between those elements on both series. Unfortunately several attempts on low loaded catalysts, *i.e.* 1Pd-0.2Cu/CZ, did not lead to conclusive information likely due to the very low concentration of those species at the surface in agreement with XPS analysis. Hence, on the basis of those observations, one can conclude that a greater proximity would characterize Pd and Cu elements in reduced 5Pd-1Cu/CZ(EISA) samples thanks to the evolution of the intensity of PdOCu⁺ cluster ions. This conclusion seems to be in rather agreement with TEM-EDS observations and with the evolution observed on the B.E. values measured for the Cu 2p and Pd 3d core levels.

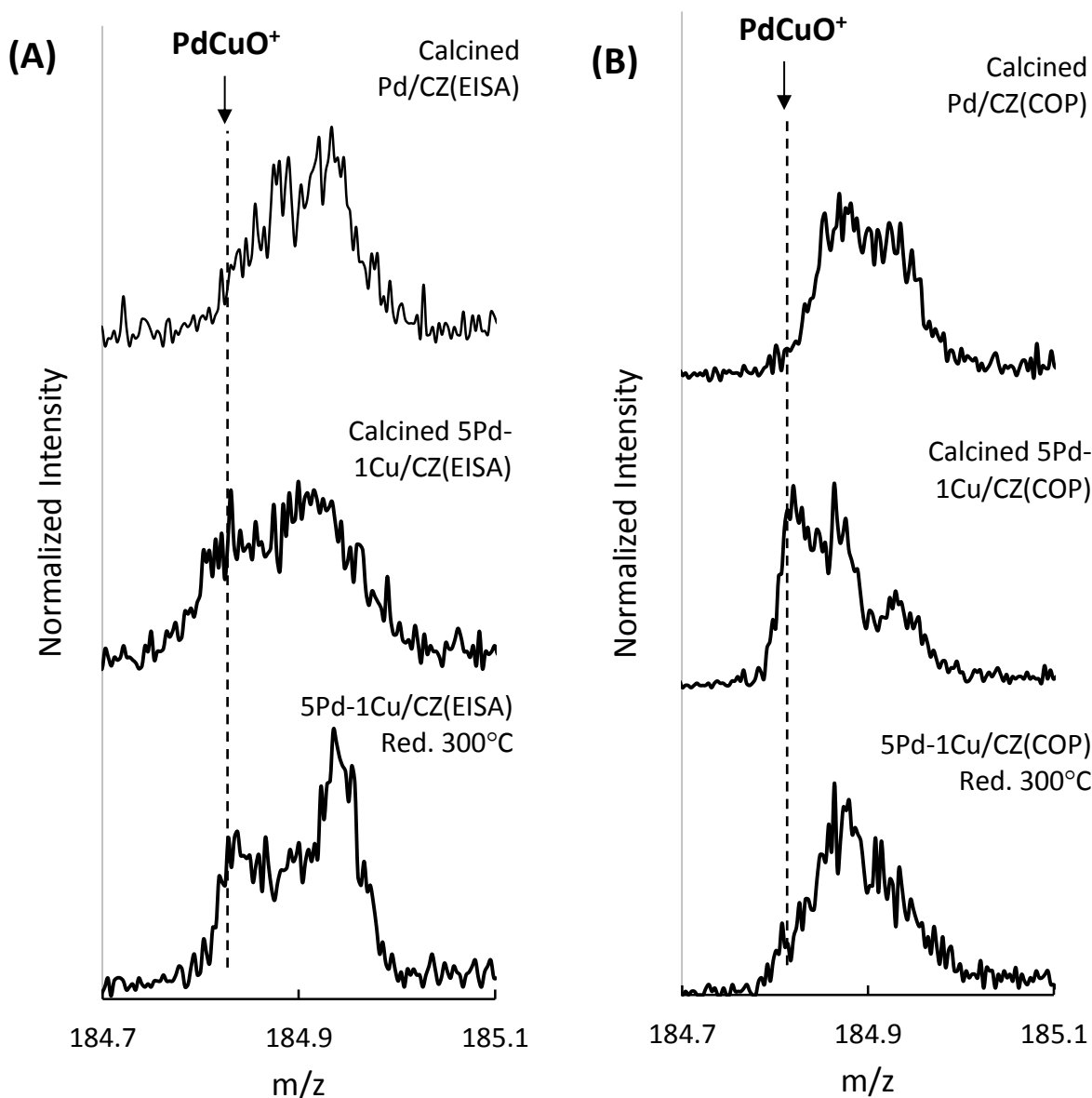


Fig. V.11. *Ex situ* ToF-SIMS analysis performed on calcined and reduced bimetallic 5Pd-1Cu/CZ(EISA) (A) and 5Pd-1Cu/CZ(COP) (B).

The cracking patterns recorded for m/z in the range 184.7-185.1 in Fig. V.12 underline an additional contribution ascribed to CuPdO^+ cationic fragments which reflects the close proximity of copper and palladium. As observed this contribution intensifies on 5Pd-1Cu/CZ(EISA).

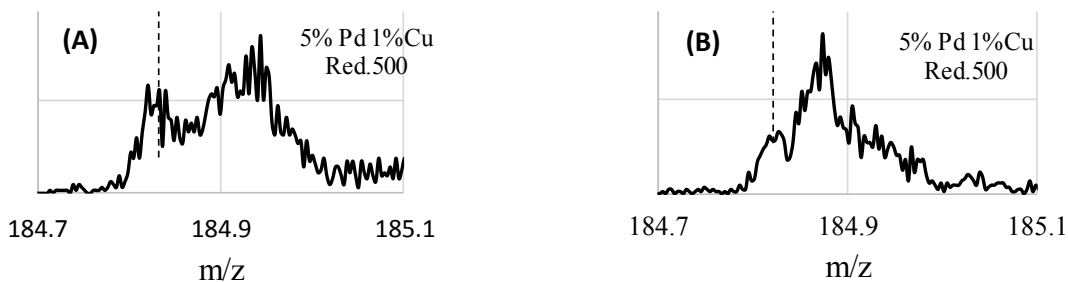


Fig.V.12. *Ex situ* ToF-SIMS analysis performed on reduced bimetallic 5 wt.% Pd – 1 wt.% Cu/CZ(EISA) (A) and 5 wt.% – 1 wt.% Pd-Cu/CZ(COP) (B) in pure H₂ at 500°C.

V.4. Discussion

Previous investigations reported that the reduction of nitrates on supported bimetallic Pd-Cu particles can depend on several parameters related to the metal loading, the atomic Pd to Cu ratio and the structure of ceria-zirconia supports[51]. We investigated the influence of the palladium loading recognized as a critical material of strategic importance by the European Union, with Pd content substantially lessened from 5 wt.% to 1 wt.%. Our kinetic measurements in batch conditions definitely show higher normalized rates of nitrates conversion on low loaded palladium catalysts, especially on 1Pd-0.2Cu/CZ(EISA). This observation is consistent with kinetic analysis leading to higher rate constant k_1 associated to the reduction of nitrates to nitrites. The lower values recorded on the series Pd-Cu/CZ(COP) could be ascribed to a greater sensibility of copper to oxidation. Another benefit associated to 1Pd-0.2Cu/CZ(EISA) is related to the lack of detection of nitrites compared to other bimetallic systems[52,53]. This behaviour suggests a much faster consecutive reduction of nitrites, *i.e.* higher k_2 than on Pd-Cu/CZ(COP). Regarding the production of ammonia at the early stage of the reaction, opposite behavior characterizes Pd-Cu/CZ(EISA) and Pd-Cu/CZ(COP) catalysts, the former being more prone to produce ammonia at high Pd loading whereas the reverse trend is observable at low Pd loading. Finally the most important discrepancy in comparing predicted and experimental curves for nitrites concentration profiles is related to an extra production over Pd-Cu/CZ(COP) which underline the occurrence of secondary reaction. All those observations underline complex surface properties depending on the degree of interaction between Pd and Cu and the peculiar properties of the support materials.

Chapter VI. Kinetics of undesired ammonia production during nitrite reduction on Pd/CeO₂-ZrO₂: Impact of metal loading and structural features of the support

This chapter was devoted to the second step associated to the reduction of nitrites on Pd/CeO₂-ZrO₂. Recently, we showed the advantages provided by the elaboration of CeO₂-ZrO₂ mixed oxides according to a soft templating method such as evaporation induced self-assembly (EISA) compared to co-precipitation methods [8,9]. The most promising catalytic performances were observed on low loaded Pd samples dispersed on CeO₂-ZrO₂ prepared by the EISA method depending on preferential interactions of Pd with the tetragonal or cubic structure of the solid solutions [9]. It was also found that this peculiar interaction can originate secondary ammonia oxidation to nitrogen whereas re-oxidation to nitrites takes place more significantly on Pd supported on CeO₂-ZrO₂ prepared by co-precipitation. A kinetic approach has been implemented in this study to understand more accurately the specific role of this type of interaction according to the preparation route of the support material to control ammonia production and especially the extra oxidation of ammonia.

VI.3.2. Kinetic of nitrites reduction and related production of ammonia

The kinetics of the overall reduction of nitrites on Pd supported on ceria-zirconia mixed oxide has been earlier reported [9]. Additional experiments were performed in batch conditions on Pd supported on single ZrO₂ and CeO₂ oxide materials to get more insights into the specific role played by the support composition which can modulate the strength of interactions with Pd particles and their related catalytic properties. Particular attention was also paid to the evolution of ammonia vs. time reported in Fig. VI.3. These observations reveal different kinetic regimes related to an instant formation and a slower consumption of ammonia. As earlier explained [14], the initial product distribution reflects the structure sensitivity of this reaction, ammonia being formed on low coordinated Pd atoms on edge and corners of Pd particles with distribution declining with a rise in Pd particle size. As a matter of fact, such structure sensitivity can be regarded because two adjacent Pd atoms are requested for the recombination of two nitrogen atoms coming from the reduction of nitrites whereas only one is needed for its subsequent hydrogenation to ammonia.

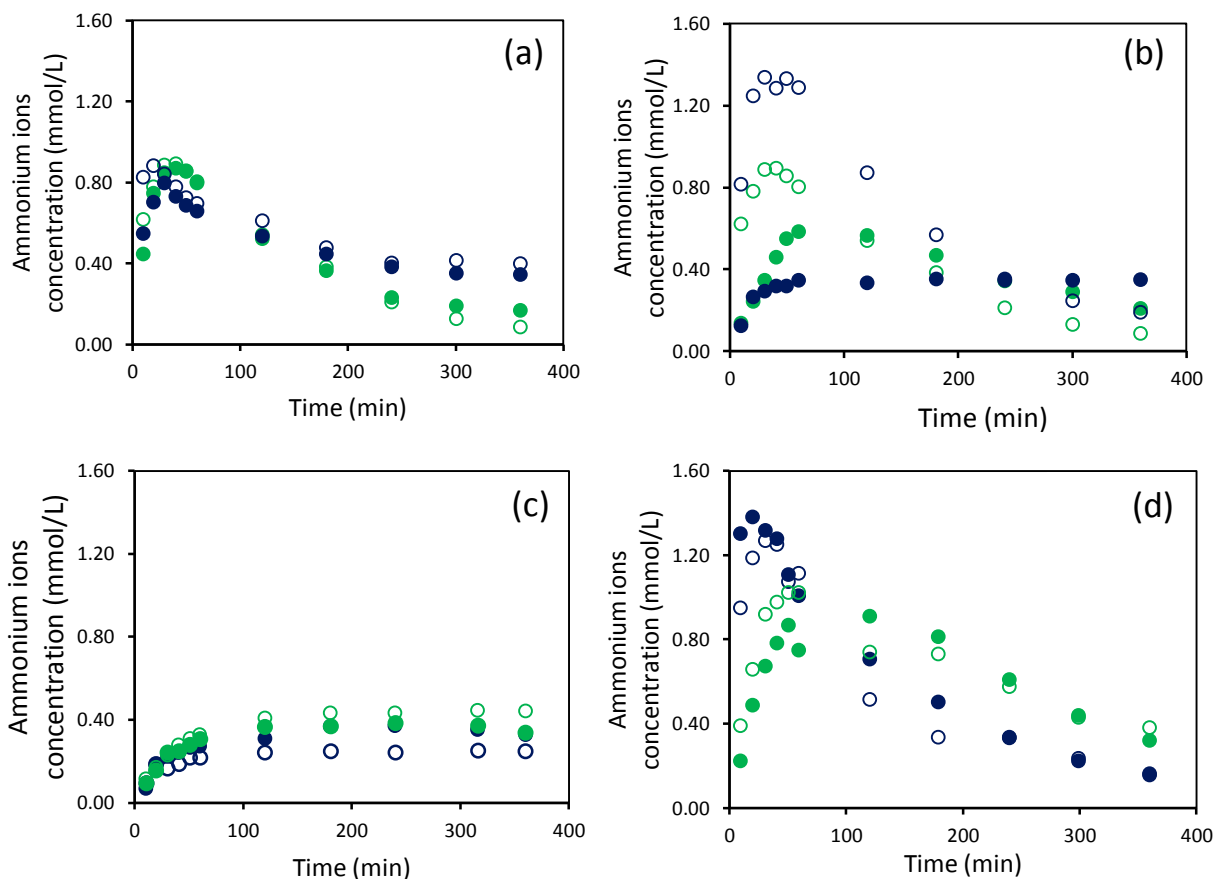


Fig.VI. 3.Concentration profiles of ammonium ions vs. time formed during the reduction of nitrites by hydrogen in batch conditions : (a) on Pd/CZ(EISA), (b) Pd/CZ(COP), (c) Pd/ZrO₂(EISA), (d) Pd/CeO₂(EISA) – full symbol reduction at 300°C, open symbol reduction at 500°C – 0.46 wt.%Pd in blue and 2.3 wt.% Pd in green.

However, in most cases the conclusions are supported by weak evidences with the hypothesis that this reaction could occur in homogeneous phase. To clarify this point, Fig. VI. 5 can be useful to state on the possible involvement of such reaction in this study.

Fig. VI.5 illustrates the evolution observed on nitrites conversion and related ammonia production[9]. As seen a fast and complete nitrite conversion takes place which corresponds to the maximum concentration of ammonium ions. Beyond this maximum a decrease in ammonium ions concentration is noticeable highlighting the occurrence of secondary reaction involving the consumption of ammonia. Previous investigations [17-19], claimed that the involvement of nitrites reduction by ammonia could occur. In our particular case, the comparison of Figs VI.5(A) and (B) rules out this hypothesis which led to the conclusion that reactive surface oxygen species from the support materials could be involved in ammonia oxidation.

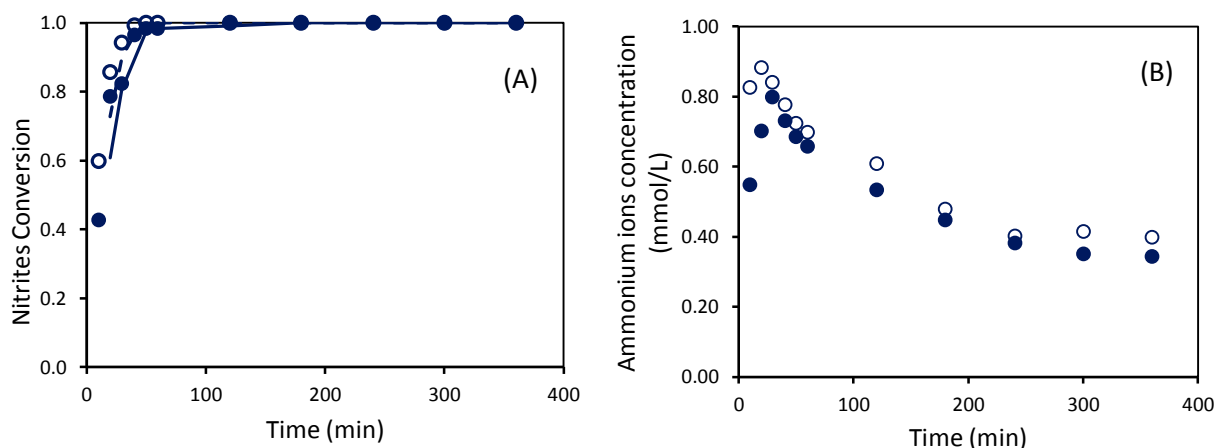


Fig. VI. 5. Nitrites conversion (A) and ammonium concentration profiles (B) vs. time on 0.46Pd/CZ(EISA) pre-reduced at 300°C – full symbol reduction at 300°C, open symbol reduction at 500°C [1].

Fig. VI. 6 provides determining argument through modeling the nitrite concentration in the course of nitrates reduction according to a two steps process with subsequent nitrites reduction to N_2 and NO_2^- . Experimental curve reveals an overproduction of nitrates assigned to ammonia oxidation. As these experiments were also performed in batch conditions and in anaerobic conditions then a point to debate is of course related to the origin of the oxidizing species involved in this process. At a first glance, the presence of trace amount of dissolved oxygen in the reaction mixture not completely degassed from water filtration could contribute to this process. However, such hypothesis seems to be invalidated by the absence of sub-oxidation observed on Pd/ZrO₂. The involvement of OSC properties of Pt/Ce_xZr_{1-x}O₂ have been already proven in Catalytic Wet Air Oxidation [20,21].

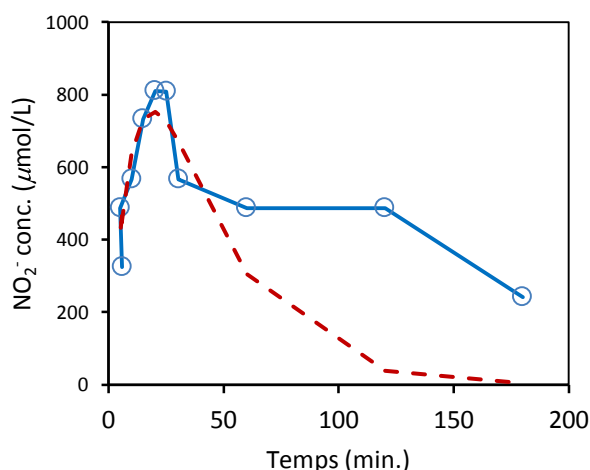


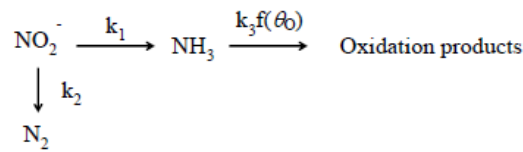
Fig. VI. 6. Predicted and experimental nitrites concentration vs. time on 1Pd-0.2Cu(COP) in the course on the reduction of nitrates by hydrogen.

By way of illustration, Yang et al. found a rate enhancement in the removal of succinic acid at increasing Ce concentration. Based on this, sub-oxidation could be intimately related to the surface density of active oxygen species as well as the metal-support perimeter. Indeed,

electron rich neighbor metallic atoms could be capable to weaken the Ce-O bond through electron transfer. Hence, observations in Fig. VI. 5 can suggest that preferential interaction between CeO₂ or Ce-riched mixed oxide and Pd in the series Pd-C/CZ(COP) and Pd/CeO₂would be more prone to oxidize ammonia. As earlier discussed [8], preferential re-oxidation to nitrites on Pd-Cu/CZ(COP) instead of nitrogenon series Pd-Cu/CZ(EISA) (not shown) could be partly explained by a lower surface anionic mobility of Zr-riched CZ(EISA) tetragonal structure compared to CeO₂ [12].

VI.3.3. Kinetic modelling

A simple kinetic model depicted in scheme VI. 1 can be envisioned for modeling the sequential formation and consumption of ammonia through reduction and oxidation reaction. One can hypothesize a pseudo first order kinetics for nitrites reduction in agreement with earlier investigations [22-24] which makes easier the resolution of the first order differential Eqs. (1) and (5).



Scheme VI. 1. Suggested parallel and sequential reactions for nitrite removal on Pd/CZ

$$\frac{d[\text{NH}_3]_t}{dt} = k_1 [\text{NO}_2^-]_t - k_3 f(\theta_0) [\text{NH}_3]_t \quad (1)$$

with $[\text{NO}_2^-]_t = [\text{NO}_2^-]_0 \exp [-(k_1 + k_2)t]$ (2)

The rate constant k_n values were estimated according to a classical least square method. The optimized rate constant values obtained when $\Sigma(r_{\text{exp}} - r_{\text{cal}})^2$ tends to a minimum are reported in Table 4. The order of magnitude for k_1+k_2 can be roughly calculated from the evolution of nitrites concentration vs. time solving Eq. (1). For ammonia consumption we have considered a pseudo rate constant which accounts for the available concentration of surface oxygen species from the support. It is worthwhile to note that the related anionic vacancies formed are not refilled in anaerobic conditions which means this reaction is not catalytic but stoichiometric. Eq. (3) from the integration of Eq. (1) is theoretically suited to model the evolution of the ammonium ion concentration vs. time.

$$[\text{NH}_3]_t = \frac{k_1 [\text{NO}_2^-]_0}{k_2 + k_1 - k_3 f(\theta_0)} [\exp [-k_3 f(\theta_0)t] - \exp [-(k_1 + k_2)t]] \quad (3)$$

The numerical values for k_1 , k_2 and $k_3f(\theta_0)$ from the adjustment routine are reported in Table 4 and then compared to those obtained according to the same method on Pd/CeO₂ and Pd/ZrO₂. Starting with Pd/CZ, at increasing reduction temperature, the rate constant k_2 as well as the sum k_1+k_2 also increase but these evolutions are not strictly related to significant changes on the ratio k_2/k_1+k_2 which reflects the selectivity to ammonia formation. The fact that the absence of correlation between k_2 and the particle size of palladium is consistent with previous statements with in connection with a weak sensibility of Pd atoms location for the hydrogenation of chemisorbed N atoms. Let us now compare these values with those calculated on supported Pd on single oxides. As a general trend, all the rate constant values on Pd/CeO₂ are usually higher than that optimized on Pd/ZrO₂ which matches the slow nitrites reduction as observed in Fig. VI.7. The values almost nil for $k_3f(\theta_0)$ on Pd/ZrO₂ underline the weak lability of Zr-O quite unreactive in our experimental conditions in comparison the Ce-O bond. As exemplified in Figs. VI. 9 a good correlation is obtained between predicted and measured ammonium ions concentration.

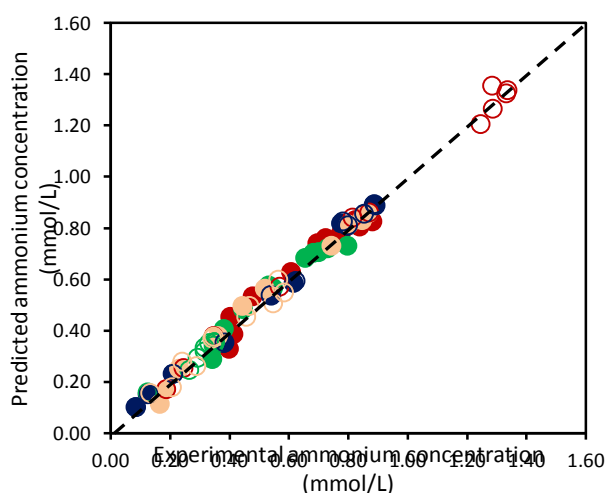


Fig. VI. 7. Correlation between predicted and experimental concentration of ammonium ions formed during the reduction of nitrites on Pd/CZ catalysts: ● 0.46Pd/CZ(EISA)-500; ● 0.46Pd/CZ(EISA)-300; ● 2.3Pd/CZ(EISA)-500; ● 2.3Pd/CZ(EISA)-300; ○ 0.46Pd/CZ(COP)-500; ○ 0.46Pd/CZ(COP)-300; ○ 2.3Pd/CZ(COP)-500; ○ 2.3Pd/CZ(COP)-300.

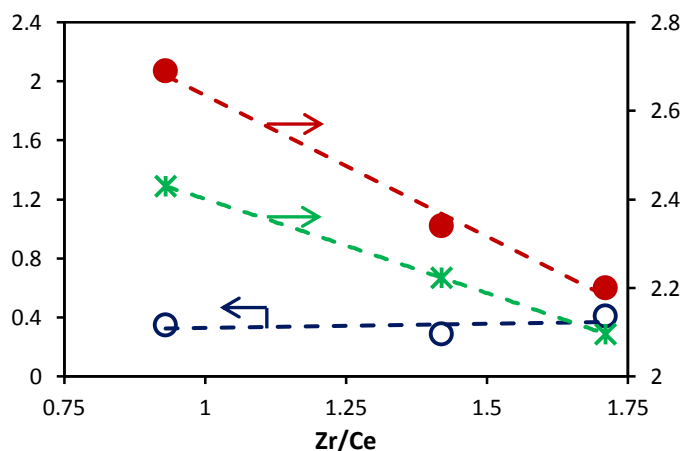


Fig. VI. 9. Correlation between surface composition and the pseudo rate constant $k_3f(\theta_0)$ (*) calculated at 300°C and the relative surface composition of oxygen O/Ce+Zr (●) and Ce³⁺/Ce⁴⁺ (○).

VI.4. Conclusions

This study dealt with the kinetics of undesired ammonia production in the course of catalytic water denitration over supported palladium catalysts on ceria-zirconia mixed oxides. Different parameters were investigated referring to bulk segregation, according to the preparation method, palladium loading and pre-reduction temperature which affects palladium dispersion. In all cases, ammonia production occurs readily but no clear comparison demonstrate a structure-sensitivity likely due to strong support effect inducing electron-rich active metallic palladium particle which could provoke an over hydrogenation of nitrites to ammonia. Interestingly a maximum in concentration profiles revealed the existence of secondary ammonia oxidation reaction. An extra oxidation of ammonia with residual nitrites has been rule out based on the comparison with different support materials exhibiting various surface oxygen mobility and related concentration. Hence, in anaerobic condition a stoichiometric reaction would involve reactive oxygen species bonded to ceria. A sequential process is proposed and catalytic exploitation from concentration profiles of ammonia vs. times led to the estimation of rate constants especially that related to ammonia oxidation which was found dependent on oxygen coverage.

Chapter VII. GENERAL CONCLUSIONS

The aim of this thesis was: i) to develop catalytic materials with an open mesoporosity in order to facilitate the transport of the reagents and products in the pores of the catalytic supports and ii) to modulate the distribution of the active phase in order to make more efficace the reduction of the nitrate.

To achieve this aim CeO_2 , ZrO_2 and mixed $\text{Ce}_x\text{Zr}_{1-x}\text{O}_2$ oxides were selected as carriers for palladium and copper, as an active phases for the catalytic reduction of nitrates to nitrogen. The efficiency of the catalyst is related in terms of :

i) concentration gradients, ii) capacity of the catalysts to avoid inhibition phenomena on the rate of reduction of nitrites/ nitrates ions and iii) effects to enhance the selectivity to nitrogen in the detriment of formation of by-products such as ammonium ions.

In summary, the results of this thesis demonstrate that the catalytic reduction of nitrate in water represents indeed an effective method to remove these. This process is strongly influenced by the chemical nature of the metal phases, the preparation method and the support. A high nitrate conversion was obtained for a catalyst with an atomic ratio noble metal/copper close to 5 treated at calcination temperature of 400 °C and reduced at 300 °C. Pd-Cu catalysts supported on $\text{Ce}_{0.5}\text{Zr}_{0.5}\text{O}_2$ showed a much superior behavior compared to

monometallic ones. In addition to high nitrate conversions for the pair Pd-Cu, the nitrogen selectivities of 76% and 82%, respectively, were obtained when $Ce_{0.5}Zr_{0.5}O_2$ has been used as a support. The reduction process of nitrates has a important time limitations. It is worth to notice that the therefore ammonium concentrations after 6 h were always higher than the allowable values in drinking water.

Selective bibliography

Chapter I

- [4] O.S.G.P.Soaes, Thesis 2010, University of Porto
- [5] EEA Report No 7/2018] <https://www.eea.europa.eu/publications/state-of-water>.
- [12] A.Kapoor, T. Viraraghavan, J. Environ. Eng.-Asce 123 (1997) 371-380
- [13] A.Pintar, Catal. Today 77 (2003) 451-465
- [16] academic.hep.com.cn
- [19] U. Prusse, K.D. Vorlop, J. Mol. Catal. A-Chem. 173 (2001) 313-328
- [33] Juan Martines, Alfredo Ortiz, Inmaculada Ortiz, Appl. Catal. B-Environ. 207 (2017) 42-59
- [37] S. Hôrold, T. Tacke, and K. Vorlop. Environ. Technol., 14 (1993) 931-939
- [38] S. Hôrold, K.-. Vorlop, T. Tacke, and M. Sell. Catal Today, 17 (1993) 21-30
- [40] Y. Yoshinaga, T. Akita, I. Mikami, and T. Okuhara, J.Catal., 207 (2002) 37-45
- [62] <https://pubs.rsc.org/en/content/articlelanding/2014/cs/c3cs60155b#!divAbstract>
- [74] www.brinkernanostructures.com

Chapter II

- [33] Sam Zhang, Lin Li, Ashok Kumar, Materials Characterization Techniques, CRC Press, 2009

Chapter III

- [24] Gu, Dong and Ferdi Schuth, Chemical Society Reviews (2014)

Chapter IV

- [14] M.-S. Kim, D.-W.Lee, S.H. Chung, J.T. Kim, I.-H.Cho, K.-Y. Lee, J. Mol. Catal. A 392 (2014) 308–314
- [23] M.A. Ebiad, Dalia R. Abd El-Hafiz, R.A. Elsalamony, L.S. Mohamed, RSC Adv. 2(2012) 8145–8156
- [63] B. Ileri, O. Ayyildiz, O. Apaydin, J. Hazardous Mater. 292 (2015) 1–8

Chapter V

- [21] N. Barrabés, A. Dafinov, F. Medina, J.E. Sueiras, Catal. Today 149 (2010) 341-347
- [23] P. Granger, S. Troncéa, J.P. Dacquin, M. Trentesaux, V.I. Parvulescu, Appl. Catal. B 224 (2018) 648-659
- [27] F. Epron, F. Gauthard, J. Barbier, J. Catal. 206 (2002) 363-367
- [42] W. Huang, Z. Zuo, P. Han, Z. Li, T. zhao, J. Electron Spectrosc. Relat. Phenom. 173 (2009) 88–95

- [43] E.M. Slavinskaya, O.A. Stonkus, R.V. Gulyaev, A.S. Ivanova, V.I. Zaikovskii, P.A. Kuznetsov, A.I. Boronin, *Appl. Catal. A* 401 (2011) 83–97
- [44] K. Otto, L.P. Haack, J.E. de Vries, *Appl. Catal. B* 1 (1992) 1–12
- [45] M. Moroseac, T. Skála, K. Veltruská, V. Matolín, I. Matolínová, *Surf. Sci.* 56 (2004) 1118–1123
- [46] P. Miquel, Y. Yamin, K. Lombaert, C. Dujardin, M. Trenteseaux, L. Gengembre, P. Granger, *Surf. Interf. Anal.* 42 (2010) 545–550
- [47] D. Das, J. Llorca, M. Dominguez, S. Colussi, A. Trovarelli, A. Gayen, *Int. J. Hydr. En.* 40 (2015) 10463–10479
- [48] M. Hronec, K. Fulajtárová, I. Vávra, T. Soták, E. Dobročka, *Appl. Catal. B* 181 (2016) 210–219
- [51] W. Gao, N. Guan, J. Chen, X. Guan, R. Jin, H. Zheng, Z. Liu, F. Zhang, *Appl. Catal. B* 46 (2003) 341–351
- [52] O.S.G.P. Soares, J.J.M. Órfão, M. F.R. P. Desalination 279 (2011) 367–374
- [53] A. Devadasa, S. Vasudevanb, F. Epron, *J.Hazard. Mater.* 185 (2011) 1412–1417

Chapter VI

- [8] P. Granger, S. Troncéa, J.P. Dacquin, M. Trenteseaux, O. Gardoll, N. Nuns, V.I. Parvulescu, *Appl.Catal. B* 253 (2019) 391–400
- [9] P. Granger, S. Troncéa, J.P. Dacquin, M. Trenteseaux, V.I. Parvulescu, *AppliedCatalysis B* 224 (2018) 648–659
- [12] S.A. Ghom, C.Z. Zamani, S. Nazarpour, T. Andreu, J.R. Morante, *Sensors and Act. B* 140 (2009) 216–221
- [14] Y. Yoshinaga, T. Akita, I. Mikami, and T. Okuhara, *J. Catal.* 207 (2002) 37–45
- [17] B. Ileri, O. Ayyildiz, O. Apaydin, *J. Hazard. Mater.* 292 (2015) 1–8
- [18] D.K. Lee, J.S. Cho, W.L. Yoon, *Chemosphere* 61 (2005) 573–578
- [19] G. Lafaye, J. Barbier Jr., D. Duprez, *Catal. Today* 253 (2015) 89–98
- [20] S. Yang, M. Besson, C. Descormes, *Appl. Catal. B* 100 (2010) 282–288
- [21] S. Keav, A. Espinoza de los Monteros, J. Barbier Jr., D. Duprez, *Appl. Catal. B* 150–151 (2014) 402–410
- [22] .M.E. Khalil, O. Eljamal, S. Jribi, N. Matsunaga, *Chem. Eng. J.* 287 (2016) 367–380.
- [23] G.C.C. Yang, H.L. Lee, *Water Research* 39 (2005) 884–894.
- [24] Z. Zhang, Z. Hao, Y. Yang, J. Zhang, Q. Wang, X. Xu, *Desalination* 257 (2010) 158–162.